DIFFUSE-TARGET FOURIER-DOMAIN HOLOGRAPHY IN PHOTOREFRACTIVE QUANTUM WELL FILMS

K. JEONG, D. D. NOLTE, M. R. MELLOCH[1]

Physics Department, Purdue University
(West Lafayette, Indiana 47907-2036),

[1]School of Electrical and Computer Engineering, Purdue University
(West Lafayette, IN 47907)

UDC 535.215

Fourier-domain holography (FDH) of diffuse targets using photorefractive quantum well (PRQW) devices has specific advantages over image-domain holography. In the recording process, the broad spatial frequencies of the diffuse target produce a broad illumination of the quantum well device that fills the device window and allows the good overlap with a broad reference profile and produces uniform modulation index across the device. This prevents the grating erasure of low spatial frequencies and hence prevents high-pass filtering. It also eliminates field screening that reduces diffraction efficiency. In the readout process, fabrication defects and dust on the quantum well film produce a delocalized low-intensity background at the readout camera as opposed to bright localized spots that occur in image-domain holography. These advantages of FDH over image-domain holography of diffuse targets make it a candidate for improved holographic optical coherence imaging applications.

Introduction

PRQW devices have achieved the first recording of depth-resolved holograms inside living tissue in a technique called holographic optical coherence imaging [1, 2]. The high sensitivity of a quantum well film makes it possible to record the extremely weak backscattered light that originates from optical discontinuities inside tissue. In these first experiments, the holography was performed in the image domain, in which the image of an object was projected directly onto the quantum well film. The reference pulse that participates both in recording the hologram and in defining the depth gate inside the tissue is also the readout pulse that is diffracted and re-imaged into a CCD camera. Dust and fabrication defects on the film scatter the reference light that is imaged directly onto the camera plane, resulting in localized "hot spots" that span the full dynamic range of the camera. This background can be partially removed by careful background subtraction, but the saturation of the dynamic range of the camera prevents long integration times to record weaker holograms coming from increasingly deeper structures inside the tissue.

Shifting the optical system to FDH removes this problem in holographic optical coherence imaging. The hologram is recorded in the Fourier-plane of the object, and the light scattered from point defects on the film is Fourier-transformed by the readout lens into a low-intensity delocalized background that is typically weaker than the reconstructed holograms. This makes it possible to use the full dynamic range of the camera, and hence to record much weaker backscattered light from inside tissue.

This paper explores the use of PRQW devices to record Fourier-domain holograms of diffuse targets, also known as speckle holography [3, 4]. Section II describes the basic principles of holography of diffuse targets, followed by section III that presents the experimental setup. The experimental results are separated into CW (long coherence) behavior in section IV and pulsed (short coherence) behavior in section V.

1. Diffuse Speckle Holography

It has been demonstrated that FDH leads to spatial filtering, which is caused by the large intensity variation at the Fourier plane, and its associated image degradation [5]. This limitation on FDH applies to a specular target but not diffuse targets such as biological tissue. Since light is diffusely scattered on diffuse targets, the sharp intensity variation at the Fourier plane is eliminated. Fig. 1 shows the schematic figure of a 4-f layout for diffuse-target FDH. Diffuse targets scatter light at the object plane and a part of the scattered beam is collimated to a recording medium at the Fourier plane by the first lens. PRQW device is used as the recording medium in our experiment. It has a finite window size and only a beam size the same as the window size is passed at the Fourier plane as shown in Fig. 1. After a hologram at the Fourier plane is recorded with the

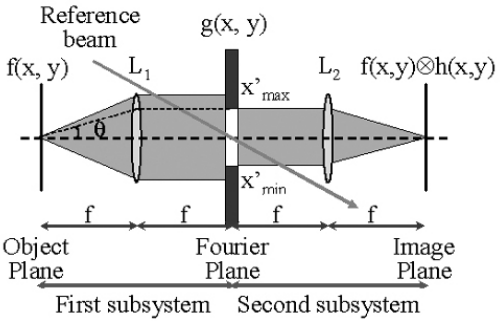

Fig. 1. Schematic figure of a 4-f layout in diffuse Fourier-domain holography. Only a part of the beam collimated by the first lens passes through the limited window size of the recording medium at the Fourier plane

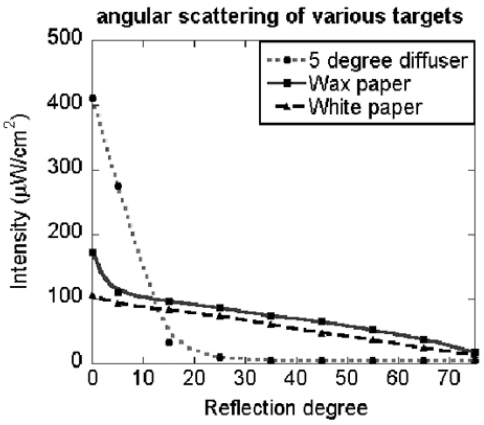

Fig. 2. Angular dependence of backscattered intensities for a five degree diffuser, wax paper, and white paper

illumination of the reference beam, the diffracted light from the recording medium forms the holographic image at the image plane by the second lens.

The wave function at the object plane in diffuse-target FDH is given by $f(x,y)$. For an ideal lens the wave function at the Fourier plane (hologram plane) is given by

$$g(x,y) = \frac{i}{\lambda f}\exp(-i4\pi f/\lambda)F\left(\frac{x}{\lambda f}, \frac{y}{\lambda f}\right), \quad (1)$$

where F is the Fourier transform of $f(x,y)$. The wave function at the image plane is $f(-x,-y)$, because the second subsystem performs an inverse Fourier transform of $g(x,y)$. When the PRQW device is used at the hologram plane, the impulse response function is given by

$$h(x,y) = \frac{1}{(\lambda f)^2}P\left(\frac{x}{\lambda f}, \frac{y}{\lambda f}\right), \quad (2)$$

where f is the focal length of the lens and P is the Fourier transform of the pupil function $p(x,y)$ of the finite window size of the PRQW device. The wave function at the image plane is then given by

$$f(x,y)\otimes h(x,y) = \iint_{-\infty}^{+\infty} f(x',y')h(x-x',y-y')\,\mathrm{d}x'\,\mathrm{d}y'. \quad (3)$$

The angular distribution of backscattered intensities at the object plane is the same as the spatial distribution at the Fourier plane in diffuse-target FDH. If the wave function after scattering at the object plane has a relatively uniform angular distribution, such as for white paper and most living tissue, the wave function at the Fourier plane also has a relatively uniform distribution. The uniform distribution of intensities at the hologram plane increases the diffraction efficiency if the reference beam is also uniformly distributed, since the diffraction efficiency is increased when the beam ratio at the recording medium is more uniform.

Randomly distributed scatterers, such as structures inside living tissue, diffuse and produce a time-varying scattered field. It is necessary to consider the anisotropic scattering that occurs due to cell structure and refractive index variations. Fig. 2 shows the angular dependence of backscattered intensities, which is obtained by measuring the backscattered intensity at a given angle when light with an intensity 6.5 W/cm^2 illuminates the surface of the scattering media. The targets were a five degree diffuser, wax paper, and white paper. The backscattered intensities are relatively uniform for white paper as also expected for living tissue.

When the scattered light is collimated to the recording medium by the first lens, the window size W of the PRQW device, the focal length of the lens, and the diameter D of the lens determine the system resolution and the collected amount of scattered light. These two values determine the numerical aperture NA of the system, which is defined by $NA = D/2f$. The cutoff frequency is given by $\nu_s = W/2\lambda f$ for the PRQW device and $\nu_s = D/2\lambda f$ for the first lens. The cutoff frequency of the system is determined by the smaller of these two values and, in our case, the PRQW window usually dominates our system. In medical applications, the collected amount of scattered light must be large to make the diffracted intensity high enough to see inside the structure because the image-bearing light in living tissue is very weak. In Fig. 1, the numerical aperture is

given by $NA = D/2f \approx \sin\theta$ for a small angle. The solid angle for the collected beam is given by

$$\Omega = \int_0^{2\pi}\int_0^{\theta} \sin\theta\,\mathrm{d}\theta\,\mathrm{d}\phi = 2\pi\left(1-\sqrt{1-\sin^2\theta}\,\right). \qquad (4)$$

The collection efficiency defined as the ratio of the collected amount to the total backscattered light is given by $\eta_c = \Omega/\pi$ when the intensity of the backscattered light depends on $\cos\theta$. The collection efficiencies are calculated to be $1.2\cdot10^{-4}$, $6.3\cdot10^{-4}$, and $2.0\cdot10^{-3}$ for the focal lengths of 9, 10, and 3.3 cm for the window sizes of 2, 5, and 3 mm respectively. The corresponding cutoff frequencies are calculated to be 1/76, 1/34, and 1/18 μm^{-1}, respectively.

The diffraction efficiency is dependent on the speckle size and the fringe spacing as well as the beam ratio. The dependence of the diffraction efficiency η_d on the fringe spacing Λ is given by

$$\eta_d \sim \left(\frac{\Lambda^2}{\Lambda_c^2+\Lambda^2}\right), \qquad (5)$$

where Λ_c is the cutoff fringe spacing. The typical cutoff fringe spacing for the current PRQW device is about 3-10 μm, and much smaller cutoff frequencies are possible using a low-temperature-growth PRQW [6]. From Eq. (5), the diffraction efficiency increases with the fringe spacing. When the signal beam with the beam size b illuminates diffuse targets, the speckle size at the Fourier plane is given by $a_s = 4\lambda f/\pi b$. The diffraction efficiency increases for larger speckle size because each speckle can support more fringes.

2. Experimental Setup

All PRQW devices used for this paper operate in the transverse-field geometry utilizing the Franz—Keldysh effect, in which the electric field is applied in parallel to the plane of quantum wells. The transverse-field PRQW devices have advantageous nonlinear optical properties over other photorefractive devices, such as high sensitivity and high-speed response due to the large absorbance and high carrier mobility of semiconductor materials [7]. The response time of these devices can be adjusted to be faster than standard video rate (30 frames/s), which makes it possible for holographic images of a moving object to be directly displayed in real-time on a video monitor.

All PRQW devices for this study have GaAs—AlGaAs multiple-quantum-well (MQW) structures grown by molecular-beam epitaxy in a Varian Gen-II

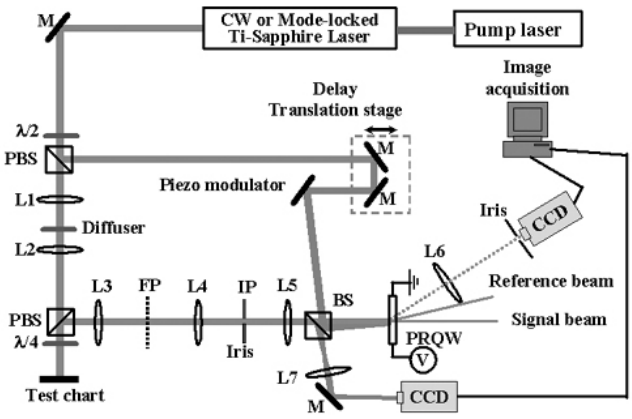

Fig. 3. The experimental setup for a CW or mode-locked Ti:Sapphire laser. PBS — polarizing beam splitter, BS — beam splitter, M — mirror, L — lens, $\lambda/2$ — half-wave plate, $\lambda/4$ — quarter-wave plate, IP — image plane, FP — Fourier plane

chamber. The MQW structure in the PRQW devices is composed of 100 periods of 7-nm GaAs wells and 6-nm $Al_{0.3}Ga_{0.7}As$ barriers, with a total thickness of 1.3 μm. During growth the MQW layer is sandwiched between 200-nm $Al_{0.2}Ga_{0.8}As$ and 250-nm $Al_{0.2}Ga_{0.8}As$ buffer layers and between 5-nm GaAs and 10-nm GaAs caps to prevent oxidation. The sandwiched MQW was deposited in a series of 10-nm GaAs, 20-nm AlAs, 500-nm $Al_{0.5}Ga_{0.5}As$, and 500-nm GaAs layers, which were deposited on a n+ GaAs substrate that was removed using the direct etching of the substrate. For the transmission-geometry PRQW, the structure was proton-implanted to make the device semiinsulating with a double dose of 10^{12}/cm^2 at 160 keV and 5×10^{11}/cm^2 at 80 keV to introduce deep defects which provide traps for photorefractive space-charge gratings. The structure was then epoxied to a glass substrate, and the semiconductor substrate was removed. Two gold contacts were evaporated on the top of the sample to apply a transverse electric field parallel to the quantum-well layers. Three PRQW devices were used to record and reconstruct holographic images. Device BH45, BH56, and JAC63 have 2-, 3-, and 5-mm window sizes, respectively.

The experimental setup shown in Fig. 3 was used to record and reconstruct holograms in the PRQW devices using either a CW Ti:sapphire laser pumped by an Argon ion laser or a mode-locked Ti:sapphire laser (120 fs pulse duration and 100 MHz repetition rate) pumped by a diode laser. The laser wavelength is tuned at the exciton peak (836 nm) for the CW laser and 836 nm with a bandwidth of 20 nm for the mode-locked laser to maximize the hologram diffraction efficiency.

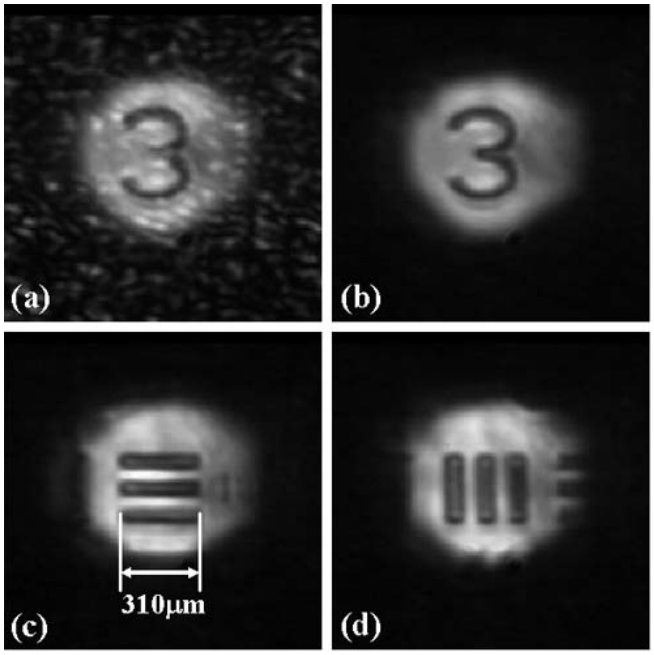

Fig. 4. Holographic images of the USAF test chart obtained using the PRQW device with 2 mm window size in a CW laser with vibrating diffuser: holographic image with background (*a*), background-subtracted holographic images (*b*)—(*d*)

The output beam from the laser passes through a first polarizing beam splitter (PBS) to produce the signal and reference beams. The half-wave plate is added before the first *PBS*, so that the reference beam has horizontal polarization and the signal beam has vertical polarization. The signal beam passes through a 4:1 demagnifying telescope consisting of lens $L1$ and $L2$ and passes the second *PBS*. A quarter-wave plate is added behind the second *PBS* so that the signal beam from the target has horizontal polarization after returning through this quarter-wave plate. After the image-bearing signal beam with horizontal polarization passes the second *PBS*, this beam is relayed with a 1:1 magnification by lenses $L3$ and $L4$. Lens $L5$ performs the Fourier transform of this relayed image at the PRQW device, where it interferes with the reference beam passing through the delay stage that adjusts to zero path. Fringes from the interference between the signal and reference beams are recorded on the PRQW device while a 10 kV/cm dc field is applied.

The hologram is reconstructed by the $+1$ or -1 diffraction orders of the reference beam and viewed in a near-IR CCD camera (Hitachi KP-F2A) using lens $L6$. The reconstructed holographic images on the CCD camera are captured by a frame grabber in the computer. Direct images of the image-bearing signal beam are captured by the other CCD camera using lens $L7$. The experimental configuration for the CW laser has essentially the same configuration as for a mode-locked laser. Lens $L6$ with a focal length of 9 cm is used for a CW laser configuration using a BH45 device (2-mm window size). Lenses $L6$ with a focal length of 3.3 cm and 10 cm are used for a mode-locked laser using the BH56 device (3-mm window size) and a JAC63 device (5-mm window size), respectively. Under CW operation, a diffuser with a diffusing angle of 1 degree, vibrating at a frequency of 42 Hz with amplitude of 1.6 mm, is introduced between lenses $L1$ and $L2$ for a specular USAF test chart to make the diffused illumination on the targets. Under pulsed operation, a vibrating mirror controlled by a piezo modulator is used for diffuse targets in the reference arm to time-average interpixel laser speckle.

3. Experimental Holography Results under CW Operation

The performance of the diffuse-target FDH system was first evaluated with a CW laser. Fig. 4 shows the holographic images of the USAF test chart obtained using the PRQW device with 2-mm window size with a vibrating diffuser. A vibrating diffuser was used to create diffused illumination on the targets so that the limitation of FDH (the large intensity variation at the Fourier plane) is eliminated. The fringe spacing was set to be 8 μm for all holographic images obtained with the CW laser, and the beam ratio (the ratio of reference beam intensity to signal beam intensity) is equal to 4 for the images in Fig. 4. The calculated resolution for this system is 76 μm and the measured resolution is 63 μm. The difference between the calculated value and the measured value results from the slight uncertainty in the position of lens $L5$ in Fig. 3. The holographic image with background is shown in Fig. 4,*a*, and its background-subtracted image is shown in Fig. 4,*b*. The maximum intensity of the background is half the maximum intensity of the diffracted intensity, and, hence, the background does not degrade the holographic image quality. Fig. 4,*c* and *d* show the background-subtracted holographic images of a horizontal bar and a vertical bar with the length of 310 μm.

When the signal beam illuminates diffuse targets, only a part of the backscattered light is collimated by lens $L3$ in Fig. 3, and only a part of this light passes the PRQW device by the limited window size. On the other hand, for specular targets, most of the backscattered

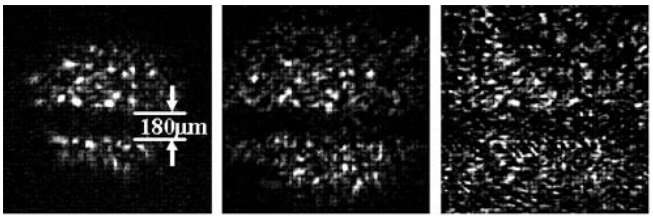

Fig. 5. Background-subtracted holographic images of diffuse paper with a horizontal cut 180 μm bar obtained with a CW laser using 0.8 (a), 1.2(b), 2 mm (c) aperture at the image plane before the PRQW device

light is collimated by lens $L3$ and passes the PRQW device. The total backscattered signal powers after passing the PRQW were measured for both diffuse paper and a specular target. The ratio of these values (the value for a diffuse target to the value for a specular target) was $5.2 \cdot 10^{-5}$. The collection efficiency for this system was calculated to be $1.2 \cdot 10^{-4}$ in section II. The difference between the calculated value and the measured value results mainly from the angular dependence of diffuse paper, as given in Fig. 2 which shows a relatively uniform angular dependence as compared with the $\cos\theta$ dependence. The total powers of the diffracted beams are also measured using the background-subtracted holographic images for diffuse paper and a specular target. The ratio of these values (the value for a diffuse target to the value for a specular target) was measured to be $8.0 \cdot 10^{-3}$. The value of $8.0 \cdot 10^{-3}$ divided by $5.2 \cdot 10^{-4}$ becomes about 150. This experimental result demonstrates that the FDH system using the PRQW device is 150 times more sensitive to a diffuse target than to a specular target. We suggest that this is due to the removal of the field screening, in which most of the applied voltage drops across the dark regions near the electrical contacts.

The diffuse-target FDH system was evaluated using diffuse white paper and a CW laser. A part of the paper was cut to form a horizontal bar with a width of 180 μm. Fig. 5 shows background-subtracted holographic images of the paper target with a CW laser using different apertures at the image plane before the PRQW device. When the aperture is used at the image plane before the PRQW device (the iris position between lenses $L4$ and $L5$), the speckle size is changed by $a_s = 4\lambda f/\pi b$, where b is the aperture size. The diffraction efficiency is changed by the speckle size as mentioned at the end in section II. The larger the speckle size (the smaller the aperture size), the higher the diffraction efficiency becomes. Fig. 5,a is for 0.8 mm aperture, b is for 1.2 mm aperture, and c is for 2 mm aperture. The speckle sizes are calculated

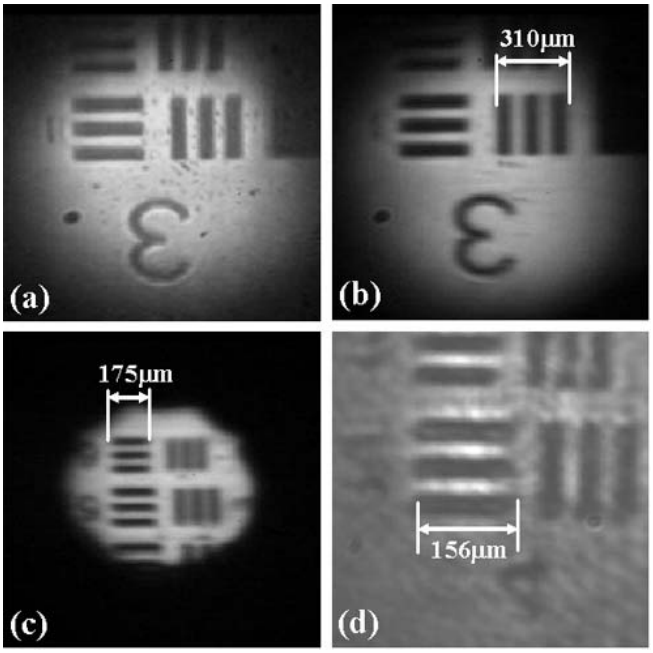

Fig. 6. Background-subtracted holographic images of the USAF test chart obtained with a mode-locked laser under CW operation (a), under mode-locked operation (b—d). a—c are obtained through the PRQW device with 5-mm window size and lens $L5$ with 10-cm focal length using a vibrating diffuser. d is obtained through the PRQW device with 3-mm window size and lens $L5$ with 3.3-cm focal length (3.6 mag) and no diffuser

to be 120 μm for Fig. 5,a, 80 μm for b. The speckle size for c is determined by the incident signal beam size, which is about 1.2 mm, and hence gives a speckle size also near 80 microns. The maximum intensity is 74 for 0.8 mm aperture, 58 for 1.2 mm aperture, and 57 for 2 mm aperture on a scale of 255.

4. Experimental Holography Results under Mode-locked Operation

A mode-locked femtosecond Ti:sapphire laser has a short coherence length of about 30 microns compared with a CW Ti:sapphire laser that has about 3 cm. This short coherence length gives a mode-locked laser an advantage to obtain a structure within the turbid medium through coherence gating. The diffuse-target FDH system was evaluated using a mode-locked laser and a specular test chart with a vibrating diffuser, various diffuse targets, and a specular test chart behind a static diffuser. Fig. 6 shows background-subtracted holographic images of the USAF test chart obtained with the mode-locked laser.

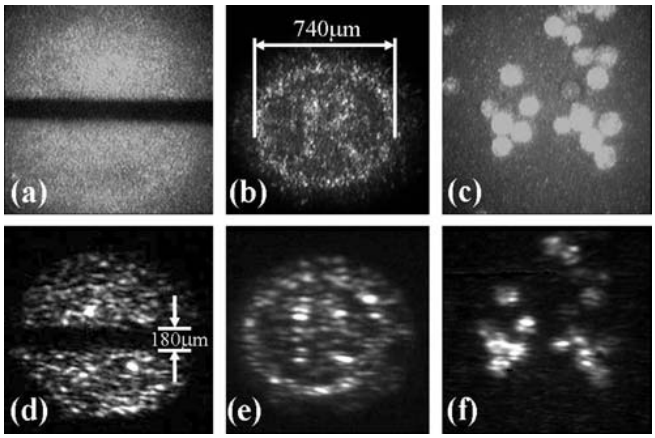

Fig. 7. Background-subtracted holographic images obtained in a mode-locked laser under mode-locked operation for diffuse paper with the cut of 180 μm horizontal bar (d) letter "R" in a circle printed with high-reflection ink on paper (e) and polystyrene beads with the size of 150 μm (f). a, b, and c are direct images for d, e, and f, respectively

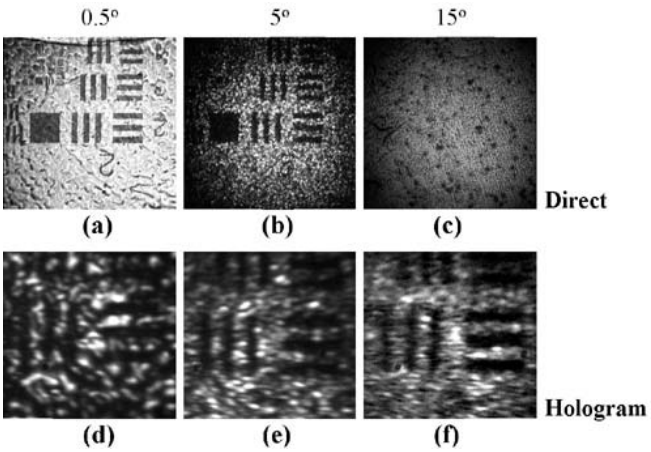

Fig. 8. Background-subtracted holographic images of a specular USAF test chart behind 0.5 (d), 5 (c) and 15 (f) degree diffuser in a mode-locked laser. a, b, and c are direct images of d, e, and f, respectively. The bars shown in holographic images have a length of 557 μm. The distance between the test chart and diffusers is about 500 μm and the thickness of diffusers is about 1 mm

A mode-locked laser can be operated under CW conditions when needed. Fig. 6,a was obtained under CW operation and b—d are obtained under mode-locked operation. Fig. 6,a—c are obtained through the PRQW device with the 5-mm window size (JAC63) and lens L5 with 10-cm focal length using a vibrating diffuser. A vibrating diffuser is again used to eliminate the large intensity variation at the Fourier plane. The resolution for this system was calculated to be 34 μm in section II. The resolution under CW operation was measured to be 35 μm. The vertical resolution was measured to be 39 μm and the horizontal resolution is measured to be 70 μm under mode-locked operation. The measured resolution under CW operation agrees with the calculated one, and the vertical resolution under mode-locked operation closely agree with the calculated one. However, the horizontal resolution under mode-locked operation is a factor of 2 smaller than the calculated one. This relates to the fringe spacing and the coherence length of a mode-locked laser. If the fringe spacing is small (the angle between reference beam and signal beam is large), the area of a zero-path matched signal beam within the coherence length will be small on the PRQW device, and, hence, the resolution will be decreased. When the fringe spacing become large or the coherence length is extended, the horizontal resolution will be increased.

Fig. 6,c shows clearly the difference of vertical and horizontal resolutions. Fig. 6,d is obtained through the PRQW device with 3-mm window size (BH56) and lens $L5$ with 3.3-cm focal length (3.6x). For this image, no diffuser was used and, hence, the edge enhancement results from a large intensity variation, as shown in the upper area of the horizontal bars in Fig. 6,d. The resolution for this system was calculated to be 18 μm and measured to be 22 μm for vertical resolution.

Diffuse-target FDH was also evaluated for various diffuse targets using the PRQW device with 3-mm window size under mode-locked operation as shown in Fig. 7. Fig. 7,d shows the background-subtracted holographic image for the diffuse paper with the 180 μm horizontal bar, e shows the letter "R" inside a circle painted using high-reflectance ink on paper, and f shows beads with 150 μm diameter. Fig. 7,a, b, and c show direct images for d, e, and f, respectively. Since the holographic image is depth-resolved under mode-locked operation, structures not matched to zero path within the coherence length are not imaged. Fig. 7,f shows that some beads in the direct image are not mapped uniformly onto the holographic image, possibly because of their lower height than other beads.

Structure inside a turbid medium can be imaged using a mode-locked femtosecond laser. The diffuse-target FDH system under mode-locked operation was evaluated to obtain the structure behind a static diffuser. Fig. 8 shows the background-subtracted holographic images of a specular USAF test chart behind a diffuser. Fig. 8,d, e, and f are obtained using a 0.5 degree diffuser, 5 degree diffuse, and 15 degree diffuser, respectively. Fig. 8,a, b, and c are direct images of d, e, and f,

respectively. The distance between the test chart and the static diffuser was about 500 μm and the thickness of the diffuser was 1 mm. It is clear that the structure behind a 15 degree diffuser could not be directly recorded, but is obtained through the holographic image using the mode-locked laser.

5. Discussion

In this paper, we have explored diffuse-target FDH in photorefractive quantum well devices for the first time as a coherent imaging technique. The technique is applicable through turbid media such as living tissue and capable of high-speed 3-D imaging and real-time acquisition of full-frame holographic images. We have evaluated this system by the obtained holographic images with good quality and high sensitivity for both a specular target and diffuse targets with a CW laser and a mode-locked femtosecond laser. We have shown that FDH has the potential to provide a significantly increased sensitivity, when this system is applied to diffuse targets. We have evaluated the change of numerical aperture, collection efficiency, and system resolution when the window size of the PRQW device and the focal length of the lens are changed. We have demonstrated that the horizontal resolution of the system is related to the fringe spacing and the coherence length of the laser. Finally, we obtained holographic images to show a structure behind static diffusers using a mode-locked femtosecond laser.

1. *Mustata P.Yu.M., French P.M.W., Turek J.J. et al.*//Appl. Phys. Lett. — 2003. — **83**. — P.575—577.
2. *Peng P.Yu.L., Mustata M., Turek J.J. et al.*//Opt. Lett. — 2004. — **29**. — P.68—70.
3. *Jones R., Wykes C.* Holographic and Speckle Interferometry: a Discussion of the Theory, Practice and Application of the Techniques. — Cambridge: Cambridge University Press, 1983.
4. *Briers J.D.*//Opt. Eng. — 1993. — **32**. — P.277—283.
5. *Jones R., Barry N.P., Hyde S.C.W. et al.*//Opt. Lett. — 1998. — **23**. — P.103—105.
6. *Nolte D.D., Melloch M.R.* //Photorefractive Effects and Materials/Ed. by D.D. Nolte. — Dordrecht: Kluwer, 1995.
7. *Nolte D.D.*//J. Appl. Phys. — 1999. — **85**. — P.6259—6289.

ГОЛОГРАФІЯ ДИФУЗНИХ ОБ'ЄКТІВ В ПЛОЩИНІ ФУР'Є У ФОТОРЕФРАКТИВНИХ ПРОШАРКАХ З КВАНТОВОЮ СТРУКТУРОЮ

К. Джеонг, Д.Д. Нольті, М.Р. Меллох

Р е з ю м е

Голографія дифузних об'єктів в площині Фур'є із використанням приладів на фоторефрактивних квантових ямах має певні переваги над голографією в площині зображень. В процесі запису дифузний об'єкт створює широкий спектр просторових частот і освітлює вхідне вікно приладу на квантових ямах широким пучком, таким чином дозволяючи добре суміщення із опорним пучком і однорідну модуляцію показника заломлення по всьому приладу. Це запобігає стиранню граток малих просторових частот і утворенню пропускного фільтра високих частот. Також не відбувається екранування поля, що зменшувало б дифракційну ефективність. В процесі зчитування фабричні дефекти і частинки пилу на плівці пристрою утворюють на приймачі камери делокалізований фон низької інтенсивності, тоді як в голографії доменів-зображень виникають локалізовані яскраві плями. Ці переваги голографії дифузних об'єктів в площині Фур'є можуть сприяти її застосуванню в удосконаленому оптичному когерентному голографічному відтворенні інформації.